

NUMERICAL INVESTIGATION ON THE EFFECTS OF TRIM FOR A YACHT RIG

Bardo Krebber¹, Krebber@naoe.tu-berlin.de
Karsten Hochkirch², Hochkirch@FRIENDSHIP-SYSTEMS.com

Abstract. This paper presents an investigation of the changes in sail forces due to different sail trim. The approach is based on a systematic variation that changes the camber and the twist of the whole sail set in four steps.

The base geometry is taken from a measured flying shape of the 10m cruiser racer sailing dynamometer of the TU-Berlin known as DYNA. A set of cameras in combination with a new in-house software provides means to record the flying sail geometry together with other data like velocity of boat and wind, heel angle and wind angle. The obtained shape is then varied parametrically and analysed numerically. Variation limits of twist and profile are given by meaningful limits as measured in the tests.

The parametric model fits the offset points of the flying shape and generates smooth and realistic surfaces of the sails. Forestay, mast, boom and the boat hull are added. This model can be updated by simply applying another sail geometry (trim) and it serves as the first part of a semi-automatic grid generation chain. A distinct topology makes it easy and fast to generate structured meshes for any trim situation to be investigated. The flow around the sails is calculated using the well-known RANS code CFX, while measured full scale wind and boat data of the basis case are used as boundary conditions. These simulations are based on preliminary studies about numerical analysis on a yacht rig.

The RANSE calculation provides a rich insight of the changes in the flow field due to trim. A closer look at the changes in aerodynamic coefficients and height of centre of effort shows that results are of realistic magnitude.

A comparison with existing analytical methods for sail force calculation shows feasible results but also problems in predicting resistance and height of centre of effort.

In addition to the existing procedures an altered analytical approach for calculating sail forces is introduced. It employs a correction for the induced drag dependent on the lift changes due to the twist of the sail and shows good correlation with the results of the RANSE calculations.

NOMENCLATURE

COE	centre of effort
Z_{CE}	height of centre of effort
Z_{CE}^{\max}	maximal height of centre of effort
Z_{CE}^{opt}	optimal height of centre of effort
AR_{eff}	effective aspect ratio
ρ	density of air at 15 °C
C_D	drag coefficient
C_{DP}	parasite drag coefficient
K_q	profile drag constant
C_L	lift coefficient
C_L^{\max}	maximal lift coefficient
r	reef-factor according to Hazen [7]
f	flat-factor according to Hazen [7]
t	twist-factor according to Jackson [9]
T	twist-factor in as introduced in chapter 7.6.
T_{max}	maximal twist factor as introduced in chapter 7.6.
T_w	twist- weight factor

1. INTRODUCTION

The performance of sailing yachts plays a vital roll in the design but also in the assessment of existing boats. Only

if the quality of the boat is known, the skill of the crew can be measured.

To gain an assessment of the performance of a sailing yacht Velocity Prediction Programs (VPP) have been developed during the last decades. These programs use the fact that a sailing yacht moving in a steady state represents an equilibrium condition and therefore the sum of all forces and moments acting at it is zero. Having mathematical models for all forces and moments these programs are able to find the optimum sailing state of the boat and predict the velocity likely to be reached.

The effects on sail forces and moments due to the trim of the sails as one component of a VPP are very complex and different approaches are currently used to model this influence.

Sailors trim their sails in order to optimise the aerodynamic forces and obtain maximum boat speed. In addition, the strain of materials are responsible for geometry changes in different load distribution. Even though the designed sail shape is basically known it is still not precisely predictable how the actual shape under certain conditions will look.

To overcome this problem this work applies real flying shapes as measured on board the TU- Berlin sailing dynamometer DYNA. This unique measuring device is based on a 10m IMS cruiser racer. In addition to force and state variable measurements, it is possible to

¹ Graduate student, Technical University of Berlin

² External lecturer at Technical University of Berlin, managing director FRIENDSHIP-SYSTEMS GmbH

reproduce the 3D sail geometry of every sailing situation measured.

In principle geometry changes brought about by the sailors can be modelled by parameters: twist and camber. Therefore a systematic variation of this two variables on a whole set of sails was carried out and the flow around the rig was analysed numerically by means of a RANSE-code.

For simplicity only the geometry of the sail was varied even though with different sail shape all other variables like heel, boat speed and wind usually change as well.

Starting with a real sailing state including flying shape, wind, heel and boat speed data assure that the origin of the variation series is authentic. Staying close enough at this origin the gradient of the resulting forces and coefficients should be realistic.

Since twist and camber are varied within the limits measured in full size, the series contains only geometries that could be realized.

2. USE OF FLYING SHAPES

The Institute of Land and Sea Transport Systems at the TU- Berlin runs a sailing dynamometer - a 10m cruiser racer designed as rig balance for force measurements [1]. In 2003 the sailing dynamometer was equipped with a set of cameras to obtain the flying shape of the sail under real sailing conditions. Eight horizontal tape stripes with 13 markers each were attached to the sails. Two photos of each sail were taken from deck and masthead simultaneously along with measurements of force, wind and other state variables of the boat. A new in-house software (3D-SAILS) identifies the markers in the photos and reproduces the 3D coordinates for each point [2] [3]. As a result of this routine a table of 3D points is available which represents the flying shape of the set of sails.

These 3D points are used for surface modelling as well as to extract the trim parameters.



Figure 1: Jib of DYNA with sail stripes and markers

3. DEFINITION OF PARAMETERS

Following common practice two variables are used:

- the camber of the sail expressed as percentage of the cord length
- the twist as the angle between the boom (or lowest cord line) and the cord lines of the sail given in degrees, Figure 2.

Analysing the data files of the sail these parameters are given for all 8 sail stripes. In order to get one single value for camber the camber is simply averaged over all sail stripes.

Because the twist increases not uniform along the height it would not be appropriate to take just the angle between the boom and the uppermost sail stripe. Here a linear best fit is introduced and the value of this line at the topmost sail stripe is taken instead. This value then constitutes the twist of the sail, Figure 3. According to this definition every set of sails consists of four parameter values i.e. two for the main and two for the jib.

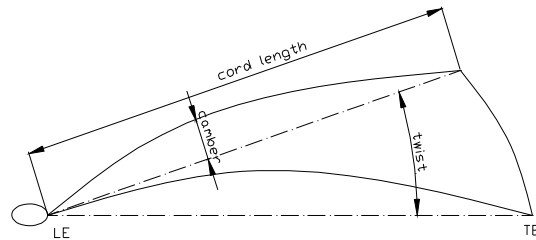


Figure 2: Definition of parameters

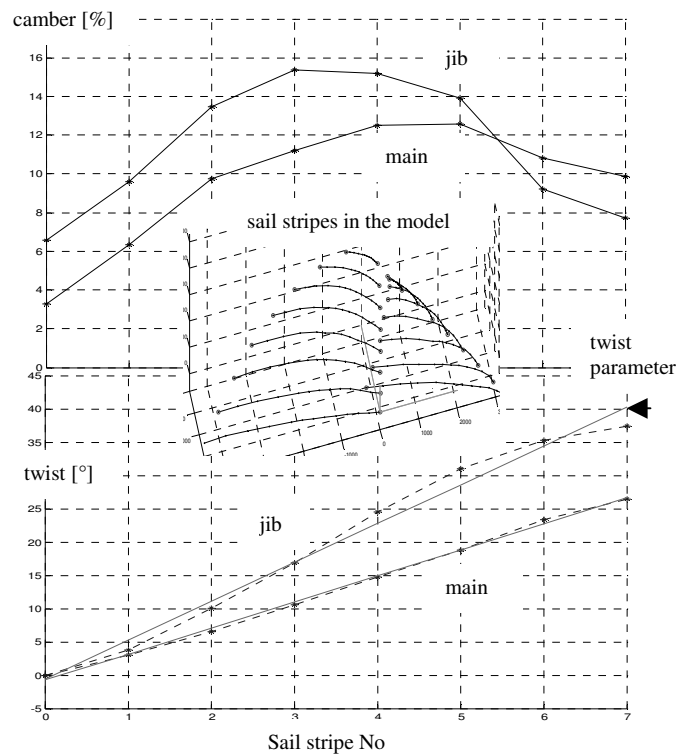


Figure 3: Typical figure of camber and twist with linear best fit along the height

4. PARAMETRIC VARIATION

Limits for the trim parameters were taken from a study of measured sailing conditions of DYNA at apparent wind angles from -30 to 30 degrees under small jib (Genoa3). By means of this criteria 37 of 480 measured cases were extracted.

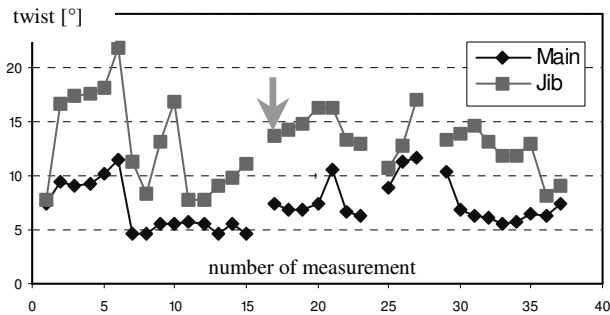


Figure 4: Preliminary analysis of twist for main and jib

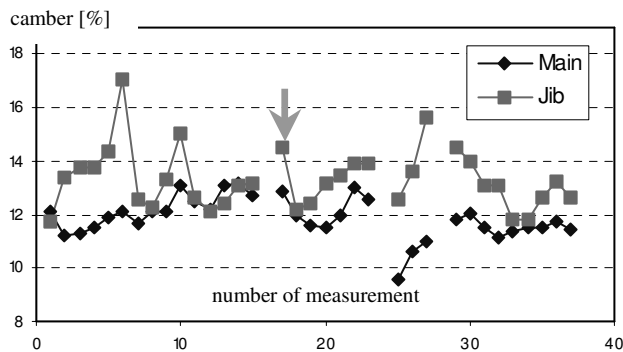


Figure 5: Preliminary analysis of camber for main and jib

As the jib is twisted far more than the main sail and operates in general with a higher camber jib and main reach different maximum and minimum values in the trim parameters. As results of a preliminary analysis twist and camber of these cases are plotted in Figure 4 and 5. The arrow indicates the chosen base case.

According to sailors the trim of jib and mainsail are supposed to be adjusted in relation to each other. Even though analysis does not show that this has actually been achieved the variation series follows this approach. Consequently parameters of jib and main are varied linearly between the corresponding upper and lower limits.

Limits have been found for every sail and every parameter individually. Maximum camber and twist of the jib and mainsail do not necessary have to occur together in the same measurement. It is of much more importance that the parameter value is physically achievable by the sail.

The base geometry is chosen to be a case with average parameters that can be considered as representative.

Wind and state variables of the basis case:

Heel	: 30.7°
Apparent wind	: 28.12° at 10.99 m/s
True wind	: 37.61° at 8.48 m/s
Boat speed	: 2.97 m/s

Camber and twist were varied linearly in four equidistant steps. This constitutes a 4 x 4 modification-matrix.

The base geometry was then modified to meet the parameters of the modification matrix. A program first

rotates and shifts the sail-stripe sections so that trailing and leading edge are in the XZ plane. To increase or decrease the camber all Y-coordinates are multiplied by a flat-factor. Subsequently the sections are rotated back by a new twist-angle that derives by multiplying the twist-angle for each sail stripe section by a twist factor, Figure 6. The required flat and twist factors are determined by simply dividing the supposed parameter value of the modification matrix by the parameter value of the base geometry. The base geometry is therefore not part of the variation series.

The so obtained shape of the sail meets the required trim parameters but differs in the sail area to some extent. However deviations are smaller than 3% of the total area.

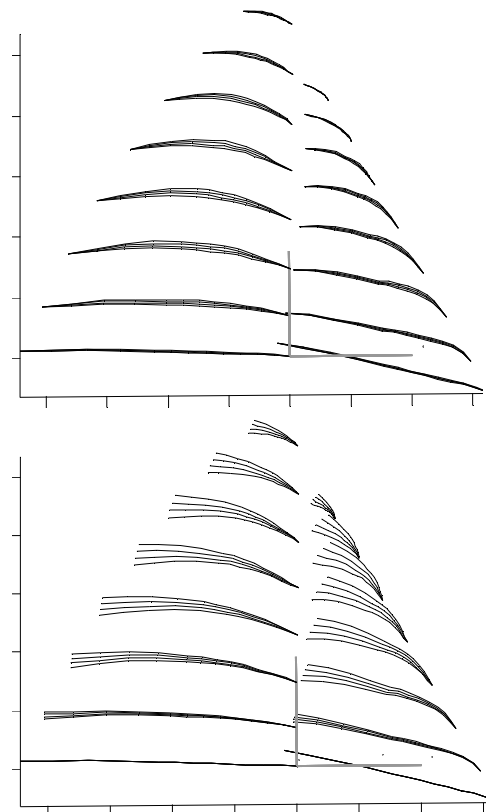


Figure 6: Variation of twist and camber

5. GEOMETRY AND MESHING

Starting from the three-dimensional coordinates of the flying shape, the geometry has to be modelled and a grid has to be generated. Due to the large number of sail shapes to be studied grid generation needed to be as automatic as possible.

A structured grid was chosen in spite of the complex geometry of the rig. Although an unstructured grid with tetrahedral cells provides much more flexibility in geometry and automatic grid generation, their use is computationally much more costly since for comparable accuracy the grid needs to have more cells. An advantage of hexahedral cells is that much larger aspect ratios can be realized. Cells can be stretched in directions with small gradients of flow quantities, e.g. along the mast.

Structured grids still can be generated automatically by using parametric positions on surfaces or curves for all vertices and edges of the grid. For this reason supplementary surfaces which stay in a relative position to the rig were introduced. How this auxiliary surfaces are applied is shown in Figure 7 using the example of the O-grid around the boom.

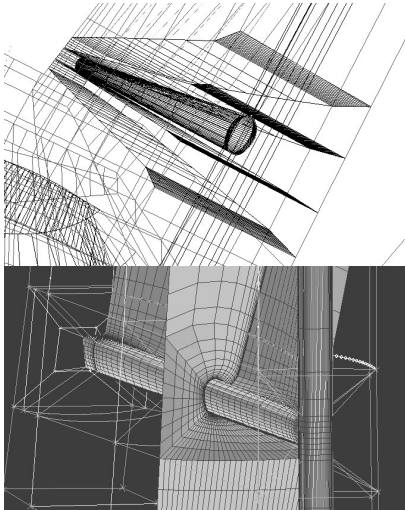


Figure 7: Utilization of assistant surfaces at the example of the boom O-grid

Cell rows in a structured grid are going through the whole domain. This causes twisted cells and small angles especially in the gaps between the sails and the deck where the sails can be hauled out overboard. General grid interfaces are employed to solve this problem. Consequently sails, boat, deck and outer grid are generated independently.

The size of the domain expands to 30m in front of the rig and to the sides, 15m above top of the mast and 60m in the wake.

Hull, deck and cabin have also been modelled. The entire geometry model with the general grid interfaces can be seen in Figure 8

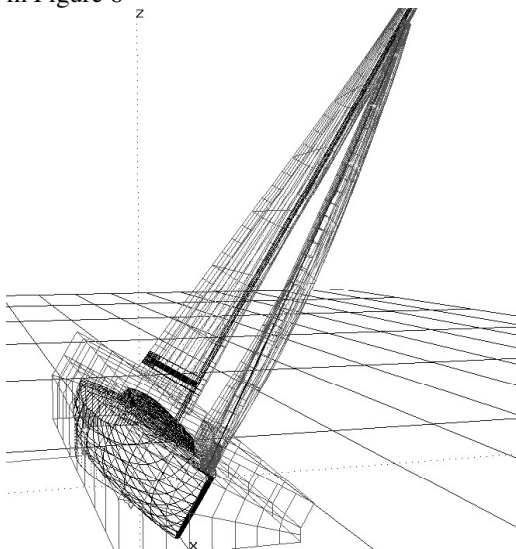


Figure 8: Geometry model

6. SIMULATIONS

The flow simulations were carried out via CFX, a general purpose RANSE code. A grid of 800 000 cells represented the fluid domain. Turbulence was modeled employing a $k-\epsilon$ approach. Steady state simulations were carried out in virtual time steps converging to constant forces after about 150 iterations in average.

Information on boat speed, apparent wind angle and wind velocity were taken from full-scale measurements. Inlet velocities were calculated combining the wind profile equation of Kervin [4] and boat speed. Streamlines in the calculated flow filed are shown in Figure 9.

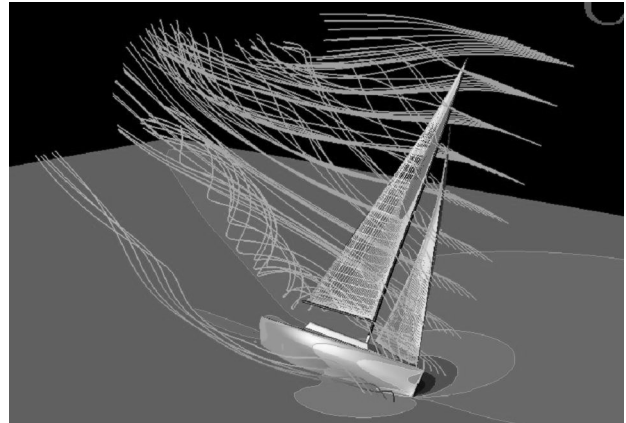


Figure 9: Stream lines and pressure distribution as result of the simulation

7. RESULTS

7.1. Coordinate systems

In CFX forces and moments are given in absolute coordinates where the origin lies in the water plane below the foot of the mainsail, X points forward, Y to port and Z upwards. The centre of effort is expressed as a fraction of mast height in a body fixed coordinate system that heels with the boat around the X axis. The leeway and the trim angle have been neglected for this investigation.

All aerodynamic coefficients are expressed in wind-coordinates. For the wind coordinate system X points towards the effective wind as described in principles of yacht design by Larsson and Eliasson [5] at the height of the corresponding centre of effort of the sails Z_{CE} . Dynamic pressure is also calculated using the effective wind at Z_{CE} .

7.2. Lift distribution

The flow field and the pressure distribution at the boundaries can be utilized to closely look at the lift along the height of the sails. Pressure has been integrated along horizontal lines projected on the sail surfaces as shown in Figure 10 and plotted over the fraction of mast height in Figures 12 and 13.

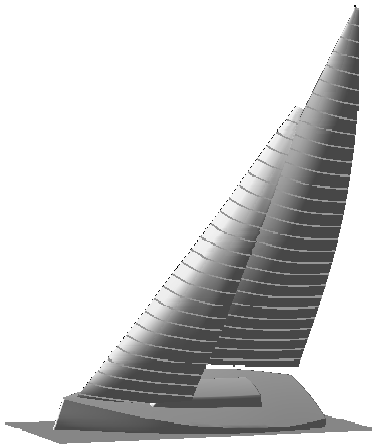


Figure 10: Lines of integration

Figure 12 shows different curves for various camber at a constant middle twist. Lift evidently increases proportional with camber over the whole span. The peak above the boom is caused by the lower tip vortex of the mainsail which takes its way at the lee side of the sail leading to higher velocity and lower pressure, Figure 11. This vortex is rather unaffected by camber.

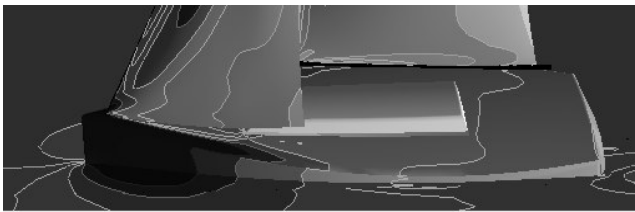


Figure 11: Pressure distribution at the lee side of the sails

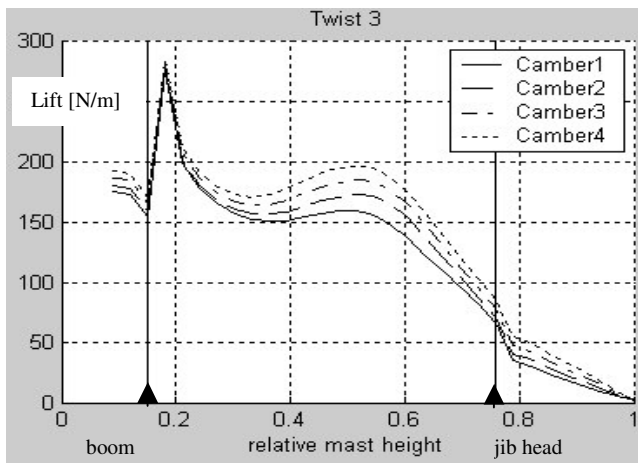


Figure 12: Change in lift distribution due to camber

Figure 13 shows the twist related changes of lift along the span at constant average camber. Higher twist causes less pressure per length at the top regions of the rig but also higher lift at the mid span. The lift at the lower sections decreases as well with higher twist. The boom vortex does not seem to vary a lot with twist either.

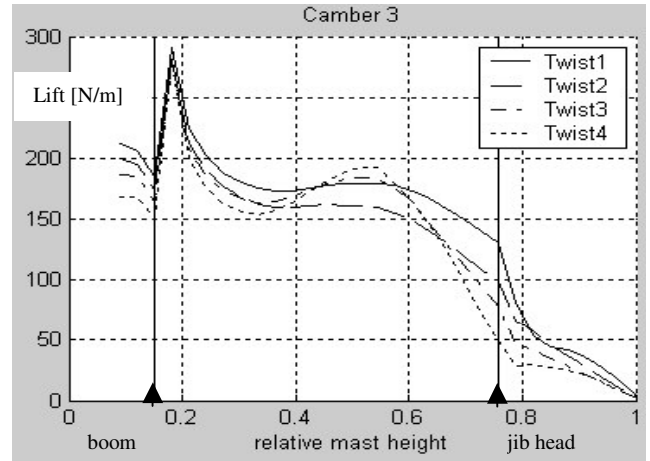


Figure 13: Change in lift distribution due to twist

7.3. Aerodynamic coefficients

Since the trim parameters are varied linearly within their feasible domain aerodynamic coefficients and centre of effort height can be plotted simply over the indices of the modification matrix. The surface shows a spline-interpolation through the 16 simulated values. Mesh grids with 16 points are introduced for comparison with values from other sources.

The lift coefficient shows an expected trend. Angle of attack for a big part of the sails is reduced when twist increases. As a result the lift coefficient reduces. Camber shows an almost linear and small influence on the lift coefficient. As a whole lift can be reduced approximately up to 50 % of the maximum by trim adjustments, Figure 14.

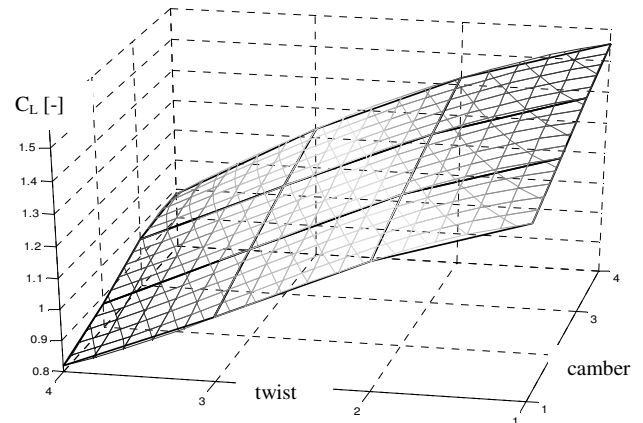


Figure 14: Lift coefficient vs. twist and camber

The drag coefficient shows also the strongest dependency when changing twist. Lifting line theory implies that the drag is coupled with the lift in a quadratic relationship and so drag should decrease with twist when the lift does. Obviously this is not true for higher twist angles. Here the constellation becomes apparently so ineffective that drag rises with falling lift. A significant minimum becomes visible. In camber direction the function seems to be almost linear. (Figure 15)

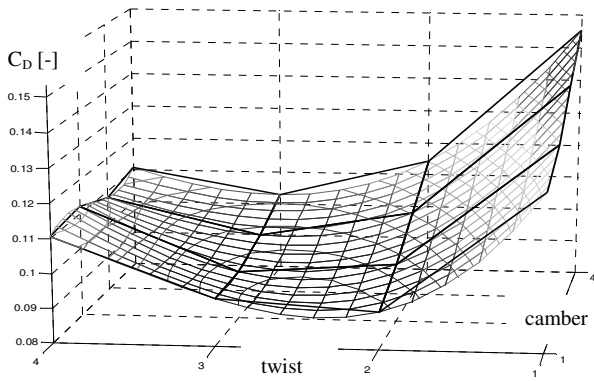


Figure 15: Drag coefficient vs. twist and camber

The height of the center of effort in body fixed coordinates as a fraction of the mast height above water (14,8 m) is shown in Figure 16.

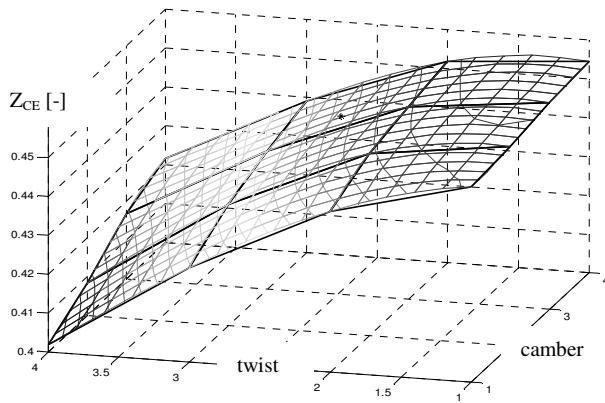


Figure 16: Center of effort height vs. twist and camber

As expected centre of effort is lowered when the sails are twisted. Change due to camber again appears to be linear. The amount of overall vertical change in Z_{CE} due to trim procedures is 5% of the mast height or 0.75 m expressed as a physical length. Not taking into account the changing lift and drag this would already yield a 12% change in heeling moment.

Figure 17 shows the tangent of the drag angle of the rig as the fraction C_D/C_L .

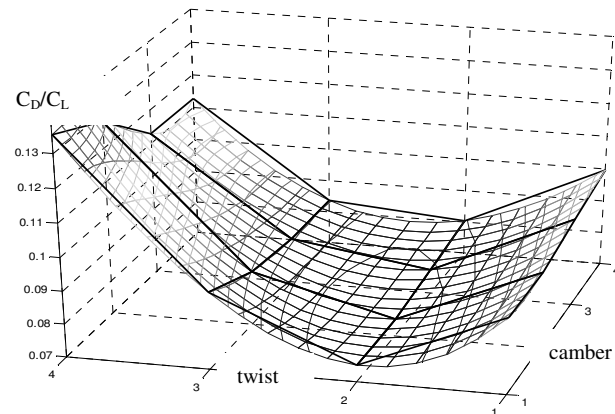


Figure 17: Tangent of drag angle (C_D/C_L) vs. twist and camber

7.4. Comparison of the results with the windage correction according to Claughton [6]

In the velocity prediction the parasite part of the drag is accounted for with a windage-correction that describes the drag coefficient of the boat's hull and the spars. This correction is made using the outline areas to the coordinate directions X and Y of each element and multiplying them with the wind velocity component normal to this areas and a corresponding drag coefficient. Drag coefficients for the hull for both directions are given with 0.68 .

Results are plotted starting from the C_D of the rig as calculated from CFD, see lower surface in Figure 18, adding the windage correction for the boat's hull. CFD-results for both the boat and the rig are shown for comparison. For perfect agreement between windage correction and CFD these two surfaces (2 and 3) should match.

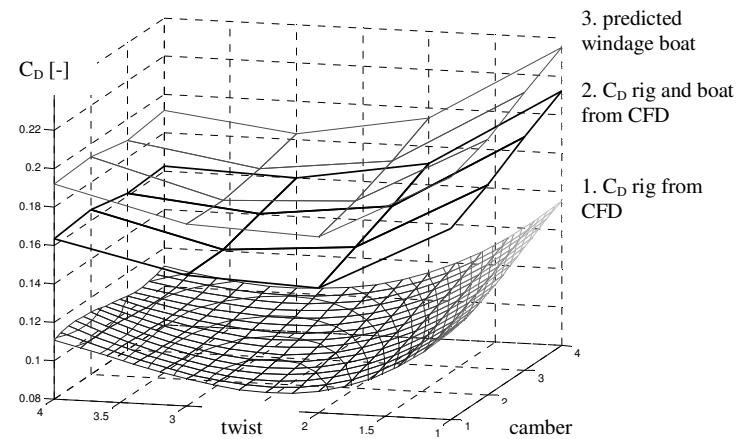


Figure 18: CFD results with windage reduction

The IMS correction for the drag of the boat does not account for the fact that the hull contributes to the lift force as well. This supportive tendency reduces the negative influence of the boat which is therefore relatively smaller than predicted, Figure 19.

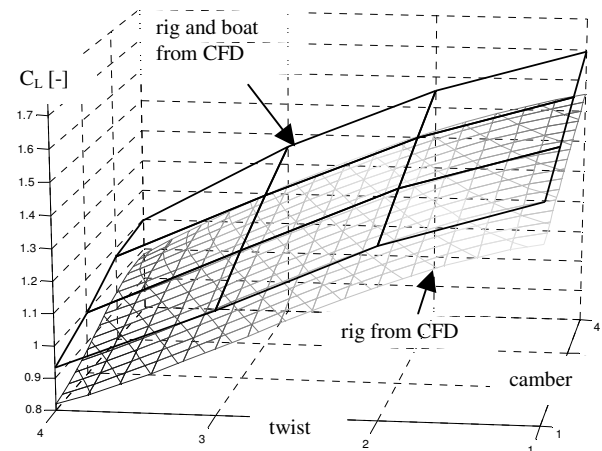


Figure 19: The boat's contributions to the lift

7.5. Comparison with models by Hazen and Jackson

A widespread and robust model which is still in use for sail force prediction was formulated by Hazen [7]. In these equations sail trim is considered by factors for reef r and flat f . Even though these factors are motivated by the actual trim done by the crew, they are not related directly to the geometry of the sails. The flat factor stands for all actions with the intention to reduce the lift of the sails apart of reefing which is represented by the reef factor. The reef factor models the reduction of the sail area and the downward shift of the centre of effort. Reef was not considered here and was therefore set to one.

The sail force equations according to Hazen read as follows:

$$C_L = C_L^{\max} \cdot r^2 \cdot f \quad (1)$$

$$C_D = C_{DP} \cdot r^2 + K_q C_L^2 + \frac{C_L^2}{\pi AR_{eff}} \quad (2)$$

$$Z_{CE} = Z_{CE}^{opt} \cdot r \quad (3)$$

For an apparent wind angle of 28° like it was used in this series the C_L^{\max} for jib and main is given in a table as 1.5. With r set to one the flat factor and the drag can be calculated using the CFD results for C_D .

Further constants are given with:

$$AR_{eff} = \frac{(1.1 \cdot H_{Mast})^2}{AS} \quad \text{Kerwin}$$

$$K_q = 0.016 \quad \text{Poor} \quad [8]$$

The drag as calculated by equation (2) shows a similar magnitude but does not correspond to the profile of the CFD results, Figure 20.

Since equation (2) is derived from lifting line theory and assumes (semi)-elliptical span wise load for the induced drag, it is not suitable for any other lift distribution as it is found in twist direction.

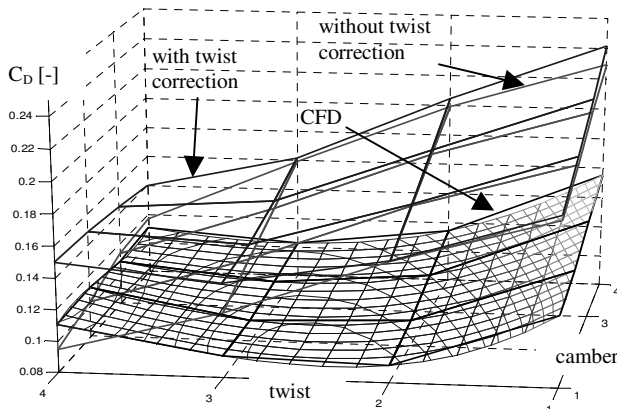


Figure 20: Drag coefficient from CFD and according to Hazen and Jackson

In order to cope with this problem the twist factor t was introduced by Jackson [9]. It models the relationship between the induced drag and the centre of effort. It is assumed that the height of the centre of effort correlates with lift distribution so that a (semi)-elliptical loading with a minimum drag occurs at an optimum height of the centre of effort. Drag is increased for a fixed lift when the centre of effort is trimmed beyond this optimum height.

The sail force equations as extended by Jackson [9] are given as:

$$C_D = C_{DP} \cdot r^2 + K_q C_L^2 + \frac{C_L^2}{\pi AR_{eff}} (1 + T_w \cdot t^2) \quad (4)$$

$$Z_{CE} = Z_{CE}^{opt} \cdot r \cdot (1 - t) \quad (5)$$

with the twist factor $t = \left(1 - \frac{Z_{CE}}{Z_{CE}^{opt}}\right)$

and the twist weight $T_w \approx 8$

Even though a sail plan with jib and main will most likely not reach elliptical or semi-elliptical loading at any Z_{CE} whatsoever (Figures 12 and 13) it is still possible that an optimum height of COE exists. This optimum height of COE which should provide the minimum drag at a given lift can be found by searching the minimum of the drag angle. It has been determined to be 44.42% of the distance between water and masthead. This implies that the COE can actually be trimmed a little higher than the optimum, see again Figure 17.

In order to achieve a visible correction in the twist-direction by Jackson's model the twist-weight factor T_w , however, had to be set as high as 100. Calculated results for equations (2) and (4) with a twist weight of 100 are shown in Figure 20 (upper mesh grid).

7.6. Equations for drag and Z_{CE} according to the results of this investigation

It is obvious that twist and camber have different influences on drag and centre of effort. The relationship between lift, drag and centre of effort due to camber seems to be practically linear whereas the variation in the twist-direction are evidently of higher order. Furthermore, the height of the centre of effort proves to be a rather sensitive parameter when calculating a drag penalty.

Consequently it has been tried to express the behaviour of C_D and Z_{CE} found in this variation series in mathematical equations by means of an extended approach. The model for the lift coefficient is extended as follows: Rather than reducing the maximal achievable lift by one factor for reef and one for everything else, at least the influence of twist should be accounted separately. This factor shall then be used to determine the Z_{CE} and a correction for the drag coefficient. Because it is relatively small and would require three extra

parameters to be identified the effect of camber can still be captured by the flat factor. The following equations show an example that approximates the data for the investigated series. Extending equation (1) the lift coefficient could be expressed as:

$$C_l = C_L^{\max} \cdot f \cdot r^2 \cdot (1-T) \quad (6)$$

whereas T is the corresponding factor for twist. It can be seen from the series that with twist 38% of the total lift can be controlled. Thus the limits of T shall be set to:

$$T \in [0, 0.38]$$

Reef r and flat f keep their original limits i.e. $r \in [0,1]$ and $f \in [0,1]$. In this constellation the flat-factor stands, in general, for variations of the lift due to different angles of attack and different camber. The results for Z_{CE} can be modelled with a quadratic term for the twist. This consideration leads to the expression:

$$Z_{CE} = Z_{CE}^{\max} \cdot r \cdot (1 - b \cdot T^2) \quad (7)$$

The parameter b is found to be 0.7. Maximum Z_{CE} still has to be given for this expression. Fortunately an inexact estimate has no effects on the drag. Even though it has not been investigated here the angle of attack should have a tangible effect on the centre of effort, Figure 21.

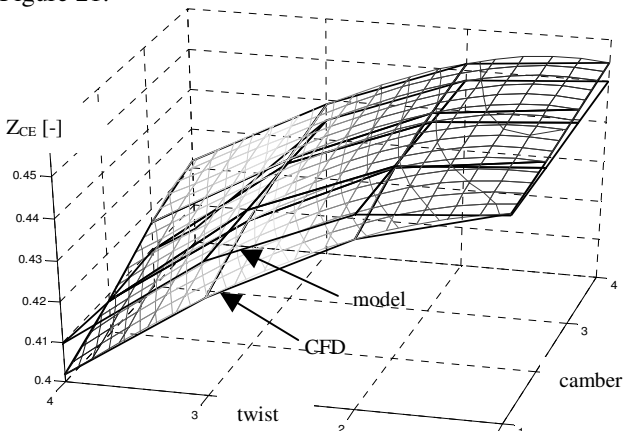


Figure 21: Z_{CE} and approximation according to equation 7

The formulation for the drag follows the familiar expression of Hazen and Jackson. To approximate the CFD results a new twist correction is added to the term for the induced drag. It incorporates the fact that an aerodynamic optimum (min C_D/C_L) have been found in the simulation. A quadratic drag penalty is applied when sails are twisted away from this optimum i.e. for all twist values that diverge from the optimum twist T_{opt} , see again the C_D/C_L in Figure 17.

$$C_D = C_{DP} \cdot r^2 + K_q C_L^2 + \frac{C_L^2}{\pi \cdot AR_{eff}} \cdot (0.3 + T_W \cdot (T - T_{opt})^2) \quad (8)$$

with the twist-weight factor $T_W = 10$
and the optimum twist factor $T_{opt} = 0.114$

A comparison of CFD data and the approximation of the model is shown in Figure 22

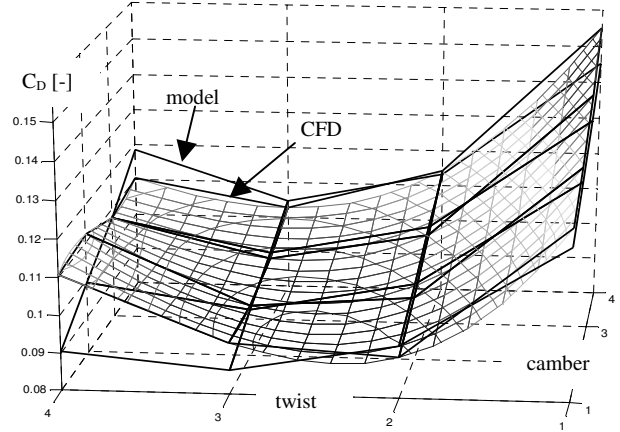


Figure 22: C_D and approximation according to equation 8

Although these equations are able to approximate the data from CFD in a reasonable way this model has still to be validated in more detail. It should therefore be understood as a proposal. Results have been backed up to some extent utilizing a subsequent series carried out with the same procedure at an apparent wind angle of 54.6° with five steps in twist and tree steps in camber. The drag minimum still has been recognized at the same position so that T_{opt} can remain at 0.114. The drag coefficient of this second series and its approximation are shown in Figure 24. It can be seen, that the drag at the upper and lower limits is under-predicted. Bearing in mind that these series is only as good as the sail shape used focus should be set to the central cases where -close to the base point- the most realistic elements of the variation occur

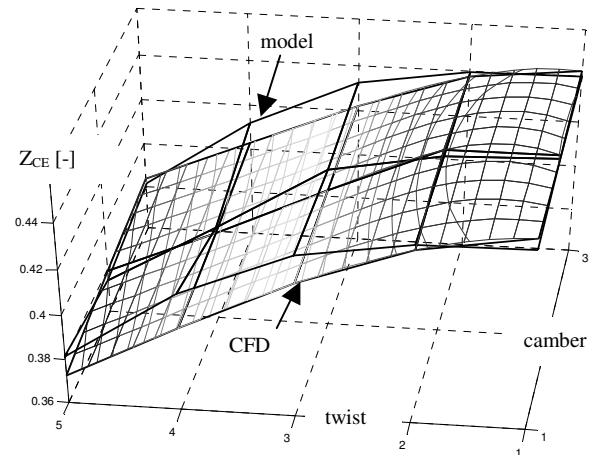


Figure 23: Z_{CE} of a second series and results from equation 7

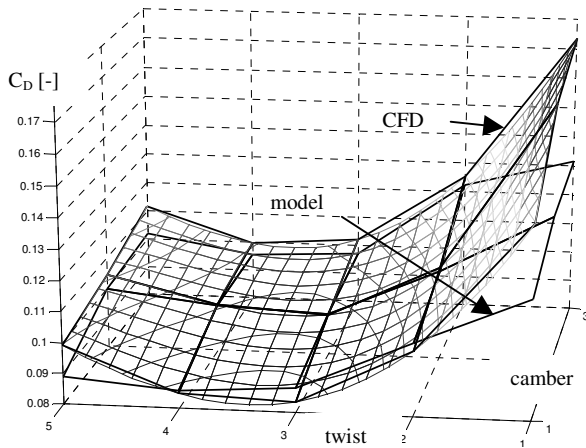


Figure 24: C_D of a second series and results from equation 8

The centre of effort varies more due to twist in the second variation series, Figure 23. Therefore, factor b from equation 7 had to be set to a higher value ($b = 1$). Presumably this factor is not constant over sheeting angles and angles of attack.

8. CONCLUSIONS

A systematic study was carried out in which two sail trim parameters – twist and camber – were varied starting from a representative flying shape. The flying shape was taken from full scale measurements performed on TU Berlin's sailing dynamometer DYNA. The flying shapes recorded gave a good indication on how far trim actually changes in operation, thus providing the limits for the variation. A parametric approach was then followed to model the flying shapes. Subsequently, the flow around the sails and the hull was simulated with a RANSE code. Although a simple method was applied, the systematic series already leads to meaningful results. It shows, for instance, that the sails can be twisted to reach a true aerodynamic optimum within given the bounds.

Existing models to calculate the aerodynamic coefficients for sail force predictions were taken to compare the CFD results of the series with existing theory. This comparison shows different characteristics. Consequently, an improved approximation by means of an extended model has been introduced. This extended model gives better correlation for the results of the systematic series

A further comparison to a second variation series that started with a flying shape at a higher apparent wind angle also gave encouraging results.

The introduced model still has to be validated in detail and should thus be seen as a proposal. A more comprehensive series and analysis of flying shapes would help to identify values and ranges of parameters in the extended model. The new model is considered to be used in a VPP for comparison with full scale measurements.

Acknowledgements

The authors would like to thank the team of the sailing dynamometer DYNA at the TU Berlin headed by Prof. Dr. Ing. G. Clauss.

Methods and adjustments of the flow simulation used in this work were preliminary investigated on a yacht rig in a thesis of Maciej Pierzynski.

Special thanks to Stefan Harries for his valuable input to this paper.

References

1. Hochkirch, K. (2000): *Entwicklung einer Messyacht zur Analyse der Segelleistung im Originalmaßstab (Design and construction of a full scale measurement system for the analysis of sailing performance)*, PhD-Thesis at Institut für Land und Seeverkehr der TU- Berlin
2. Muenster, J. (2005): *Modellbasierte Bildinterpretation zur 3D Objektrekonstruktion von Segelprofilen*, Masters-Thesis at the Institut für Informatik und Elektrotechnik der TU- Berlin,
3. Clauss, G & Heisen, W, (2005) CFD analysis on the flying shape of a modern yacht rig, *Proceedings of Maritime Transportation and Exploration of Ocean and Costal Recourses*, Lisbon
4. Kervin, J.E. (1987): A velocity prediction program for ocean racing yachts revised to February, 1978 *Technical Report 74-17, Massachusetts Institute of Technology*
5. Larsson, L & Eliasson, R.E. *Yacht Design and Konstruktion (Principles of yacht design)*, Delius Klasing Verlag 1998, Germany
6. Claughton, A.(1999) Developments in the IMS VPP formulations, *Proceedings of The Fourteenth Chesapeake Sailing Yacht Symposium*
7. Hazen, G.S. (1980): A model of sail aerodynamic for diverse rig types, *Proceedings of New England Sailing Yacht Symposium*
8. Poor, C.L (1986) A description of the new international rating system, *Publications of the United States Yacht Racing Union (USYRU)*
9. Jackson, P. (2001) An improved upwind sail model for VPPs, *Proceedings of The 15th Chesapeake Sailing Yacht Symposium*